Modelling Mechanical Enhancements in Competitive Cycling

P. Cangley[*], L. Passfield[#], H. Carter[*], M. Bailey[*]

[*] Chelsea School
University of Brighton
Eastbourne, BN20 7SR, UK
e-mail: p.cangley@brighton.ac.uk

[#] Centre for Sports Studies
University of Kent
Chatham, ME4 4AG, UK
e-mail: l.passfield@kent.ac.uk

ABSTRACT

A 3D cycling model has been developed that combines bicycle mechanics, rider biomechanics and environmental factors into a single dynamic system. The aim of the model is to identify mechanical mechanisms that influence performance in a road cycling time trial with simulations representing real cyclists competing over an actual course.

The model is constructed using the Matlab toolbox SimMechanics to model physical entities and Simulink to model control structures. The system is actuated by force or motion actuators applied to joints or bodies with sensors measuring the resulting forces and motion. SimMechanics automatically derives the equations of motion leaving the developer free to concentrate on defining the mechanics of the system. Initial conditions are specified and a variable step ODE solver numerically integrates solutions that meet defined tolerances.

Initial validation compared model simulations with data reported in the literature. Rider-less self-stability after a perturbation was found to compare well with previous work. Weave eigenvalues became negative at 4.2 m/s and capsize eigenvalues became almost positive at 6.1 m/s. Crank torque over a cycle at 255 W was recorded from the model and found to correlate well (R^2=0.97) with previously published experimental data. Finally, the tyre model generated tyre cornering stiffness of 62N/degree which closely matched the 60 N/degree reported by a previous investigation.

Experimental field validation compared actual and model predicted time taken by 14 experienced cyclists to complete a time trial over an undulating 2.5 mile road course. The course was digitised and loaded into the model and the model parameterised with individual mass and aerodynamic characteristics. Wind strength and direction were also measured. An error level of 1.4% (±1.5%) was found between actual and predicted time. This compares well with the average 1.32% error reported by existing road cycling models over less complex courses.

Keywords: modelling, cycling, bicycle, forward dynamics.

1 INTRODUCTION

The bicycle has been extensively modelled since invention of the safety bicycle by John Starley in 1885 (Wipple [1]; Carvallo [2]; Roland [3]; Meijaard et al. [4]). More recently, the cyclist has been modelled in respect of pedalling (Hull and Jorge [5]; Redfield and Hull [6]; Neptune and Hull [7]) and upper body motion (Soden and Adeyefa [8]; Stone and Hull [9]) but in isolation from bicycle dynamics. A few studies have modelled the environmental aspects of field cycling but with the bicycle/rider as an inert point mass and pre-specified propulsive/resistive forces (Olds [10]; Swain [11]; Martin et al. [12]). No published study has been identified which com-

bines the bicycle, rider and environment into a single dynamic system which is necessary if competitive field cycling is to be modelled effectively.

A large number of mechanical variables influence the performance of a competitive cyclist requiring extensive field testing if optimal combinations are to be identified. Alternatively, modelling enables a limited number of potential optimisations to be identified prior to field investigation. Models that simulate the mechanics of sport typically utilise either inverse dynamics or forward dynamics methods. An inverse dynamics model inputs motion data captured from video or measurement of an athlete performing the action and then calculates the resulting forces that drive a simulation. Although an effective method, inverse dynamics is usually limited to accurately predicting results under the conditions that applied at the time of the recorded motion. A forward dynamics model constructed from mechanical first principals should be developed if a generalised model is required that reproduces performance under a wide range of conditions. However, model accuracy will be influenced by initial approximations and assumptions prior to experimental validation.

The purpose of the study presented here is to describe a comprehensive mathematical model for optimising performance in road cycling. Components of the model are validated by comparison with previous studies and the complete model is validated by field experiment. These validations are intended to show that the model can be used to identify mechanical developments which will enhance the performance of competitive cyclists.

2 MODEL OUTLINE

The model is constructed using the Matlab toolbox SimMechanics to model physical entities and Simulink to model control structures. The main sub-systems comprising the model are shown in Table 1. In SimMechanics, a 'machine' is built using blocks to represent rigid bodies linked by joints (including closed loops). Rigid bodies and joints are linked with lines that essentially represent 2-way 'action-reaction' physical connections providing implicit inertial effects in a complete system. Simulink also uses a block and connecting line system although in this case the blocks represent logical/mathematical functions and connecting lines carry data. The system is actuated by force or motion actuators applied to joints or bodies with sensors measuring the resulting forces and motion. A range of constraint blocks allow limits to be placed on forces/motions and provide functions such as gears and rolling wheels.

Table 1. Main Model Components

Bicycle (Trek Madonne)	Rider (Typical 70 kg)	Environment (Course G10/42)
16 rigid bodies with dimension/mass/inertia	14 body segments (from literature)	Course track (from digital map)
Freedoms: x y z translation; roll, pitch, yaw rotation; steering/cranks/wheels rotation	Symmetrical two legged pedalling	Course gradient (from aerial laser mapping)
Holonomic + non-holonomic wheel constraints	Cyclic vertical/horizontal pedal force (phased 180°)	Bicycle/rider aerodynamics
Tyres (slip/camber forces, aligning/overturning moments)	Synchronised bicycle-rider roll	Environmental wind speed/direction
Geometry (COM, steer axis, trail, wheelbase)	Balance, counter-steering and path following	
Transmission	Torso and arm rotation	
Frame + wheel flex		

The model in this study is constructed hierarchically with the top level shown in Figure 1. Subsystems are implemented for areas such as tyres, transmission, path tracking and bicycle/rider (Figure 2). The lowest level in the hierarchy is a single block representing a rigid body (Figure 3). Block parameters include mass, inertia tensor, centre of gravity, dimensions and initial orientation with respect to global or local coordinate systems. SimMechanics automatically derives the equations of motion for the complete system leaving the developer free to concentrate on defining the mechanics of the system. Initial conditions are specified and a variable step ODE solver numerically integrates solutions that meet defined tolerances. The developed system operates in forward dynamics mode where forces applied to the model result in motion subject to constraints.

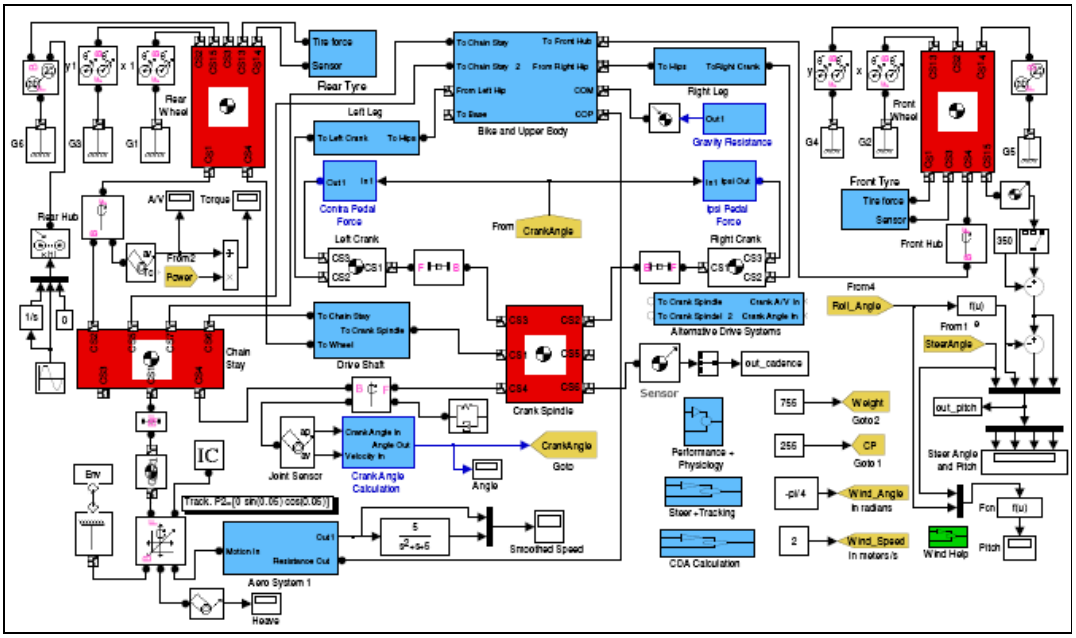

Figure 1. Top level model hierarchical organisation

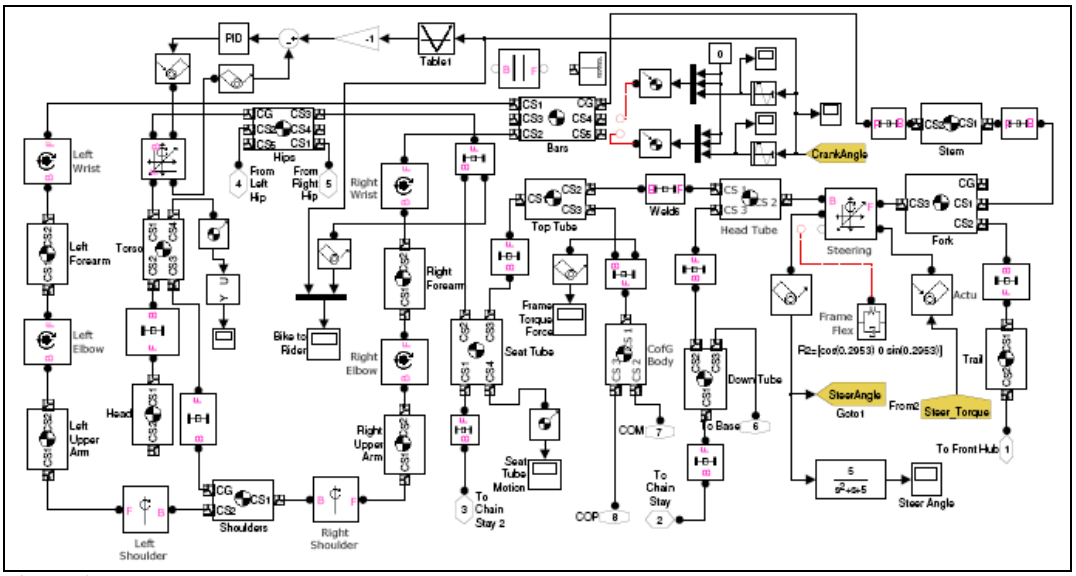

Figure 2. Second level model hierarchical organisation

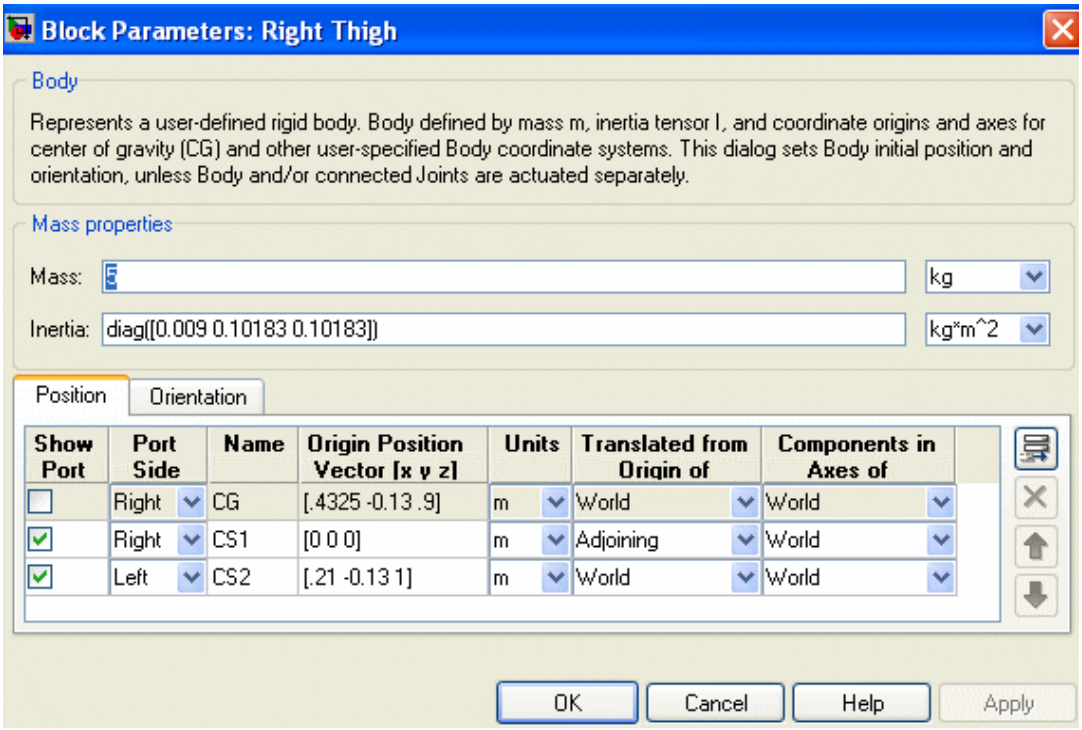

Figure 3. Bottom level model hierarchical organisation

3 BICYCLE STRUCTURE

3.1 Configuration

The model is configured with a right handed orthogonal coordinate system comprising longitudinal x axis, lateral y axis and vertical z axis. When the system is viewed from the rear, the positive axis orientations are: x = forward, y = left and z = up. The bicycle and rider are laterally symmetrical about the xz plane with the left side being defined as contra-lateral and the right side as ipsi-lateral. Additionally a right handed steering axis is orientated positively upwards. The global origin is located at the rear wheel/ground contact point and gravity acts downwards

at 9.81 m/s/s. The bicycle has degrees of freedom (DOF) for longitudinal, lateral and vertical translation, roll, yaw and pitch rotation, plus rotation of the steering, chainring/cranks and both wheels. The bicycle reference configuration is stationary, upright, straight ahead with the ipsi lateral crank arm at top dead centre (TDC). The centre of mass (COM) for the combined bicycle/rider is identified by a force balance. The longitudinal COM is found by balancing the system about the z axis. Gravity is then changed to act longitudinally and the system re-balanced about the x axis followed by iterative z and z axis balancing to arrive at a stable COM. The centre of pressure (COP) is approximated from measurement of the bicycle/rider frontal area as presented by the SimMechanics visualisation tool with segment mass areas displayed. The centre point of the area is then calculated.

3.2 Bicycle Frame

The dimensions and mass of the bicycle are based on measured values for a commercially available Trek Madone bicycle of size 59. A front and rear frame are specified with the rear frame comprising six rigid bodies modelled as tubes plus the rear wheel. The front frame comprises handle bars, stem, fork and front wheel and is connected to the rear frame by a steering joint with its axis inclined at 72 degrees to the left horizontal. SimMechanics allows separate rigid bodies to occupy the same physical space without penalty and therefore only one seat stay, chain stay and fork are modelled and placed on the bicycle longitudinal centre line. The mass of each body was obtained by weighing or by reference to the manufacturer's specifications. The inertia tensor of each body was derived from its dimensions, mass and shape/density using algorithms provided by SimMechanics. Flexibility is built into the frame by enabling the steering joint to additionally rotate about the x axis. A spring/damper is placed on this additional joint to control the level of flex to manufacturer specifications.

3.3 Wheels

Both wheels are modelled as knife edge rigid discs rotating about a revolute hub joint. The inertial mass of each wheel is distributed evenly between the hub and the rim utilising SimMechanics algorithms for a rotating disc. Wheel lateral flexibility is implemented by enabling additional hub rotation about the x axis with the level of flex being controlled by a spring/damper to meet manufacturer specifications. Wheel rotation and translation are related by a non-holonomic constraint which enforces pure rolling without slip while holonomic constraints control each wheel's relationship to the ground. A sine function implements wheel (and frame) vertical oscillation which simulates road surface plus tyre vertical compliance. The tyres are not modelled in a physical sense but the forces and torques generated by the front and rear tyre are derived analytically and applied to the wheel hub (see Tyre Model below).

3.4 Transmission

A laterally orientated crank spindle is located in the bottom bracket of the bicycle frame and rotates about the y axis. Crank arms are welded at 90 degrees to each end of the crank spindle and opposed at 180 degrees with conceptual pedals at the end of each crank arm. A gear wheel is fitted to the crank spindle which engages with a gear wheel orientated at 90 degrees fitted to a rotating drive shaft running longitudinally from the crank spindle to the rear axle. A further gear is fitted to the rear end of the drive shaft which engages with a gear on the rear axle to complete the transfer of propulsive torque from the crank to the rear wheel. The number of teeth on the gear wheels can be adjusted to set the overall gearing ratio. This system can more easily be implemented in SimMechanics than a chain drive and incurs no measurable penalty (the drive shaft mass is minimised and co-exists on the bicycle centre line with the chain stay).

A gear system has been developed based on a car automatic gearbox which is currently implemented on a static bicycle prior to inclusion in the full model. It incorporates two planetary gear sets that provide four forward gears, engaged with a series of clutches that make use of the SimMechanics 'stiction' facility. The gear box mass and dimensions are miniaturised without loss of functionality and inserted into the centre of the drive shaft. Any effect on the bicycle dynamics is minimal.

4 BICYCLE BALANCE AND STEERING

4.1 Balance

The model implements gravity and therefore the bicycle must be actively controlled to remain upright. This is achieved with a PID which attempts to maintain zero roll by applying a steering torque in the direction of any fall. Inputs are coordinated with a second PID that applies steering torques to track a defined path (see below).

4.2 Steering

Steering is currently implemented by a joint torque applied at the steering axis linking the front and rear frames. Future systems will implement steering via force applied by the rider's arms on the handlebars. The effects of the steering function are dominated by the front frame geometry which has the steering axis inclined at 72 degrees to the left horizontal. A critical parameter is the trail which is defined as the distance between the steering axis intersection with the ground and the front wheel ground contact point. The trail value is a key quantity relating the roll and steer necessary to keep the bicycle upright due to its influence on the degree of front end pitch that occurs with steering. The model provides an easily adjustable trail by parameterising the wheelbase value which moves the front wheel contact point relative to the steering axis ground intersection. The trail should properly be adjusted by also changing the steering axis but this is impractical in the current model and the effect of the omission is considered negligible.

4.3 Path Tracking

The bicycle follows a path defined by Ordinance Survey eastings and northings. The bicycle is initially aligned with the northings and as it proceeds, deviations from the required eastings are corrected by steering inputs. For the field validation, northing/easting coordinates for the first 2.5 miles of the G10/42 time trial course were captured from a digital map. The height of each coordinate was obtained from Google Earth as Ordinance Survey values were found to be insufficiently accurate. A commercial source of height data accurate to 1 m (obtained by laser mapping) was identified but not utilised for this study due to cost. A sub-system monitors the bicycle position along the northing coordinate at each time step and obtains the required easting coordinate from a lookup-file which interpolates between the measured intervals. The error between the required and actual easting position is then corrected by application of steering torque. A PID controller with appropriate gain values controls the torque to minimise the error. All bicycle position sensing (translational and rotational) is implemented about a single point situated at ground level mid-way between the front and rear wheel contact points.

5 RIDER STRUCTURE

The rider is constructed from 14 rigid bodies as shown in Table 2.

Table 2. Rider Segments

	Segments	Number of Segments
Leg (x 2)	Thigh, Shank, Foot	6
Arm (x 2)	Upper Arm, Forearm	4
Upper Body	Pelvis, Torso, Shoulders, Head	4

The dimension, mass and inertia tensor of each segment are obtained from literature (Redfield and Hull [6]) or calculated by SimMechanics. The hips are fixed to the top of the bicycle seat tube, the forearms are fixed to the handle bars and the feet are fixed to the pedals. Segments and

their inertia tensors are symmetrically distributed about the sagittal plane. The leg and arm segments are linked by revolute joints enabling rotation about the y axis (excepting the shoulders and hips which are modelled by spherical joints). The torso and pelvis are linked by a revolute joint enabling upper body lateral rotation about the x axis.

Each leg together with the seat tube and crank arm comprises a closed loop 5-bar linkage with two DOF. The crank angle controls one freedom while the other is controlled by an interpolated look-up file which specifies the ankle angle at each degree of crank rotation. The ankle angle profile (which is approximately sinusoidal) is obtained by digitising a profile presented in the literature (Redfield and Hull [6]). Pedalling has been implemented for validation purposes on a static bicycle by the application of joint torques at the ankle, knee and hip. This is planned for transfer to the dynamic bicycle at a later stage.

Few cycling models implement upper body forces and motion which are likely to significantly affect performance. In the current model, a PID controller leans the upper body about the x axis in opposition to the bicycle roll generated by pedalling in order to maintain the ensemble COM above the wheelbase taking into account the centripetal effects of cornering. Currently upper body rotations about the y and z axes are not included. An important development will be implementation of rider force application to the handlebars in opposition to the pedalling downstroke. These forces are significant at high power levels and are applied in both vertical and longitudinal directions by each arm (Stone and Hull [9]). Steering is currently activated by torque applied directly to the steering joint but is being developed to implement a couple applied by the arms to the handlebar ends. Riding out of the saddle is not currently planned due to the problem of accurately simulating body motion.

6 PROPULSIVE/RESISTIVE FORCES

6.1 Propulsive Force

The bicycle/rider is propelled by the application of vertical and horizontal force profiles to each pedal over a cycle. Forces for the contra-lateral pedal are implemented as 180 degrees offset to the ipsi-lateral pedal. Force profiles were obtained from instrumented pedal measurements on an ergometer in this laboratory (Bailey et al. [13]) for power values of 130, 200, 270, 340 and 410 W. Vertical and horizontal forces at each one degree of crank angle for each power level and each pedal were loaded into a 2D look-up matrix that applies an interpolated force value from input of a power level and crank rotation position.

The torque generated at the crank spindle is transmitted to the rear wheel as specified in the transmission section above. Cadence resulting from the specified torque and power is currently uncontrolled pending installation of the gear system described above. In the interim, the course gradient and the defined power values result in a cadence range of 70 to 115 rpm which is considered acceptable. An initial-condition velocity of 8 m/s is necessary to achieve this cadence range which is implemented in field trials by a rolling start.

6.2 Resistive Forces

Aerodynamic and gradient resistances are modelled analytically and applied in the x and y axes of the global coordinate system at the bicycle/rider COP (aerodynamic) and COM (gravitational) respectively. Rolling resistance is incorporated in the tyre model while inertial resistance due to acceleration requires no explicit modelling as it is an inbuilt consequence of the SimMechanics physical design. Transmission frictional losses are ignored as power is measured at the rear wheel

6.2.1 Aerodynamic Resistance

The model applies the following expression relating aerodynamic resistance to apparent air velocity (calculated as the sum of air velocity induced by bicycle motion and environmental wind):

$$F_{Ax} = 0.5 \cdot p \cdot CDA \cdot V_x^{\,2}$$
$$F_{Ay} = 0.5 \cdot p \cdot CDA \cdot V_y^{\,2} \quad (1)$$

where the x and y subscripts denote the longitudinal and lateral axes respectively, F_A is the aerodynamic resistive force, V is the apparent air velocity, p is the air density and *CDA* is the coefficient of drag area (drag x frontal area). Initial values are set at p=1.22 kg.m^3 (typical sea level) and *CDA*=0.37 with the latter being modified dynamically throughout a simulation by the calculated wind yaw angle to the bicycle direction of travel (Martin et al. [12]; Kyle [14]). The yaw angle of the bicycle from the right horizontal is monitored to ensure the resistive forces are applied as values opposing motion (which can be negative or positive in the x or y axes depending on the bicycle direction).

6.2.2 Enviromental Wind

The induced air velocity is modified by both the speed and direction of the environmental wind. Environmental wind strength and direction are specified by initial values although both can vary during a trial if a known profile is available. The model re-calculates wind effect at each time step as the track direction changes. The effect of environmental wind on aerodynamic resistance is calculated by first resolving the wind vector into x and y axis components with the following expressions:

$$V_{Wx} = V_W \cdot \cos W_\theta$$
$$V_{Wy} = V_W \cdot \sin W_\theta \quad (2)$$

where V_W is the wind velocity and W_θ is the wind angle from the right horizontal. The resolved components are then subtracted from the induced air velocities measured on the appropriate x or y axis to arrive at the apparent air velocities for each axis.

6.2.3 Gravitational Resistance

SimMechanics enables gradient resistance to be applied in a physical sense but the gradient value cannot be changed during a simulation. Since the gradient changes frequently in the experimental validation, resistive forces must be calculated and applied analytically. Resistance is computed from the following expression:

$$F_G = M \cdot g \cdot \sin(\arctan(G_R)) \quad (3)$$

where F_G is the gravitational resistive force, M is the ensemble mass and g is the force due to gravity. The bicycle/rider is not rotated about the y axis to reflect the gradient as the effect on pedalling has been found to be minimal (Caldwell et al. [15]). The resistive force is resolved into x and y axis values and then applied in opposition to the ensemble direction of travel at each time step.

7 TYRE MODEL

7.1 Introduction

The handling and path-following of a bicycle are substantially influenced by the behaviour of two relatively small contact patches linking the tyres to the road, making an accurate tyre model critical to the fidelity of bicycle performance. If a bicycle is to turn, the two tyres must provide

equal and opposite inwards forces opposing the conceptual 'centrifugal force' acting outwards. More exactly, the centripetal acceleration into a turn is driven by the magnitude of the lateral tyre force. Tyre slip and wheel camber provide this lateral force without which the bicycle response to a steering input would be to continue straight ahead (familiarity with tyre dynamics theory is assumed for this section).

Few studies have experimentally investigated bicycle tyres requiring data to be inferred from other single track vehicle studies, principally those relating to the motorcycle. However, despite the extensive motorcycle tyre literature (Cossalter et al. [16]; Lot [17]; Pacejka [18]), motorcycle characteristics diverge from the bicycle in a number of areas such that comparisons should be made with caution. In particular, bicycle competitive speeds averages 25-30 mph compared to 100+ mph for motorcycles, bicycle/rider mass is typically 85 kg compared to 350 kg for the motorcycle/rider, bicycle tyre width is 23 mm versus 120 mm for a motorcycle and bicycle tyre pressure is typically 100-130 psi compared to a motorcycle's 30-40 psi. Finally, a bicycle's large diameter spoked wheels exhibit significantly greater flex than the smaller motorcycle alloy casting.

A transient step-change steering input has been selected to exercise the tyre model as it highlights the temporal development of tyre forces/moments compared to a more progressive steering control. In a competitive sport context, the chosen manoeuvre equates to a cyclist changing direction to exploit a gap during the final sprint of a road race (also similar to the initial action of the 'lane change' manoeuvre often used in vehicle testing).

7.2 Model Structure

Two sub-systems generate front and rear tyre forces/moments respectively in response to motion inputs. Tyre slip angle and lateral tyre force are calculated respectively from:

$$\alpha = \arctan\left(\frac{V_y}{V_x}\right) \qquad (4)$$
$$F_y = C_\alpha \cdot \alpha + C_\gamma \cdot \gamma$$

where α is slip angle, V_y is wheel lateral velocity, V_x is wheel longitudinal velocity, F_y is lateral force, C_α is cornering stiffness, C_γ is camber stiffness and γ is camber angle. The first term in the lateral force equation calculates slip force, the development of which is lagged by a first order lag function with a time constant equal to relaxation length divided by speed. The second term calculates camber force which is not lagged in this derivation. Aligning moment and overturning moment are calculated respectively from:

$$M_z = C_{m\alpha} \cdot \alpha + C_{m\gamma} \cdot \gamma \qquad (5)$$
$$M_x = F_z \cdot \delta_c$$

where M_z is aligning moment, $C_{m\alpha}$ is aligning moment stiffness, $C_{m\gamma}$ is aligning moment camber stiffness, M_x is overturning moment, F_z is vertical tyre force and δ_c is vertical force lateral offset due to camber. Only aligning moment is lagged and calculated as for slip. Rolling resistance is calculated as $\mu \cdot m \cdot g$ where m is bicycle/rider mass, g is the gravitational constant and μ is the rolling resistance coefficient obtained from an experimental 'coasting-down' test.

7.3 Tyre Parameter Identification

The identification of tyre parameters is critical to model fidelity and appropriate values should be obtained from experimental testing. However, no tyre test facilities were available for this study and therefore tyre parameters are estimated from experimental measurement of bicycle tyres reported in the literature. These are summarised in Table 3.

Table 3. Bicycle Tyre Parameters (* = parameter utilised in the model)

	Meijaard & Schwab [19]	Limebeer & Sharp [20]	Cole & Khoo [21]	Roland & Lynch [22]	Sharp [23]
Cornering Stiffness (N/rad)	Front=1,500 Rear=2,500	4842	3,553	3,680*	Front=4,430 Rear=8,778
Camber Stiffness (N/rad)		338		49	Front=309* Rear=613*
Aligning Moment (Nm/rad)					Front=71* Rear=176*
Overturning Moment (Nm/rad)					-0.31 at 5° camber*
Vertical Stiffness (N/m)		150,000		125,787-178,165	
Vertical Load (N)		338	329	338	Front=309 Rear=613
Rolling Resistance Coefficient				0.0068	
Relaxation Length (m)		0.1*			Front=0.021* Rear=0.028*
Contact Patch Length (m)		0.1			Front=0.12 Rear=0.13
Pneumatic Trail (m)	Front=0.012 Rear=0.018			0.003	Front=0.016* Rear=0.02*
Crown Radius (m)	Front=0.015 Rear=0.02			0.02	0.01

Variances are considerable in the values reported above due to differences in test conditions and applied parameters. These differences were analysed in detail to identify the values most appropriate for this study with the selected parameters being marked by an asterisk in Table 3.

Only one study in Table 3 reports a rolling resistance coefficient, which is surprising given that R/R can generate significant resistance to motion particularly at the lower speeds incurred during hill climbing. A study by Kyle [24] contains the most comprehensive experimental tyre testing that can be identified in respect of tyre type, surface and inflation pressure (the later two factors in particular being key components of the R/R coefficient). The study reported a coefficient of 0.004 for a 23 mm clincher tyre at 95 psi rolling on smooth tarmac and this value has been adopted in the cycling model.

7.4 Model Assumptions

The lateral force/slip angle relationship is assumed to be linear as slip angle can be expected to remain below 5 degrees in a time trial (Gillespie [25]). Longitudinal slip is neglected as the magnitude of acceleration and braking force is assumed to be negligible in a time trial. A 'thin-disk' wheel/tyre is modelled and the effects of tyre width are accounted for in the equations of motion rather than through physical tyre dimensions. Overturning moment due to side slip is also neglected (Blundell and Harty [26]). Tyres are assumed to be axially symmetric with no plysteer or conicity effects requiring bias correction at zero slip angle (Roland [3]). A nominal vertical tyre load is applied based on a force balance apportioning total bicycle/rider weight between the front and rear tyres.

7.5 The Simulation

The full cycling model is simulated from rest and accelerates upright and straight-ahead to reach a steady-state speed of 11.1 m/s after ~7.5 s. A transient steering input is applied at ~7.9 s comprising a step-input of 4 degrees to the right generating a bicycle yaw rate of 40 degrees/s with subsequent steer/roll inputs returning the bicycle to upright equilibrium on a new track at 9 s when the simulation is terminated. Forces, moments and motions for front and rear tyres are recorded at the simulation time-step frequency (~0.01 s) enabling results to be graphed and analysed. All results are presented as absolute values since force generation consumes energy regardless of tyre orientation with respect to any particular axis.

7.6 Results

Tyre output data measured by the simulation and resulting derived values are shown in Table 4. Only the period containing pronounced steering motion from ~7.9 s to 9.0 s contributes significantly to the results.

Table 4. Tyre Outputs from a 4° Steering Step-Input

	Front Tyre	Rear Tyre	Total Tyres	Comment
SLIP FORCE				
Peak Slip Angle (degrees)	2.2	3.0		
Peak Slip Force (N)	130	187		
Peak Yaw Velocity (deg/s)	112	44		
Peak Slip Power (W)	228	73		
Slip Work-Done (J)	8.4	7.7	16.1	82% of Total
CAMBER FORCE				
Peak Camber Angle (degrees)	2.9	4		
Peak Camber Force (N)	17	27		
Peak Roll Rate (deg/s)	101	95		
Peak Camber Power (W)	20	18		
Camber Work-Done (J)	1.5	2.0	3.5	18% of Total
SLIP + CAMBER FORCE				
Peak Power (W)	230	91	276	
Work-Done (J)	9.8	9.8	19.6	
ALIGNING MOMENT				
Peak Moment (N.m)	2.4	8		
OVERTURNING MOMENT				
Peak Moment (N.m)	0.2	0.3		

Note. Peak power, force and velocity values are not directly related due to timing differences.

7.6.1 Lateral Force due to Slip Angle

The 4 degree initial steering input generates a front slip angle of 2.2 degrees and a peak lateral force of 130 N when tyre cornering stiffness is 3680 N/rad and vertical load 338 N (Figure 4). When combined with a front wheel yaw velocity that peaks at 112 deg/s, a peak power of 228 W is transferred from forward propulsion to lateral propulsion. Integrating the power profile over the simulation shows that the power transfer represents 8.4 J of work.

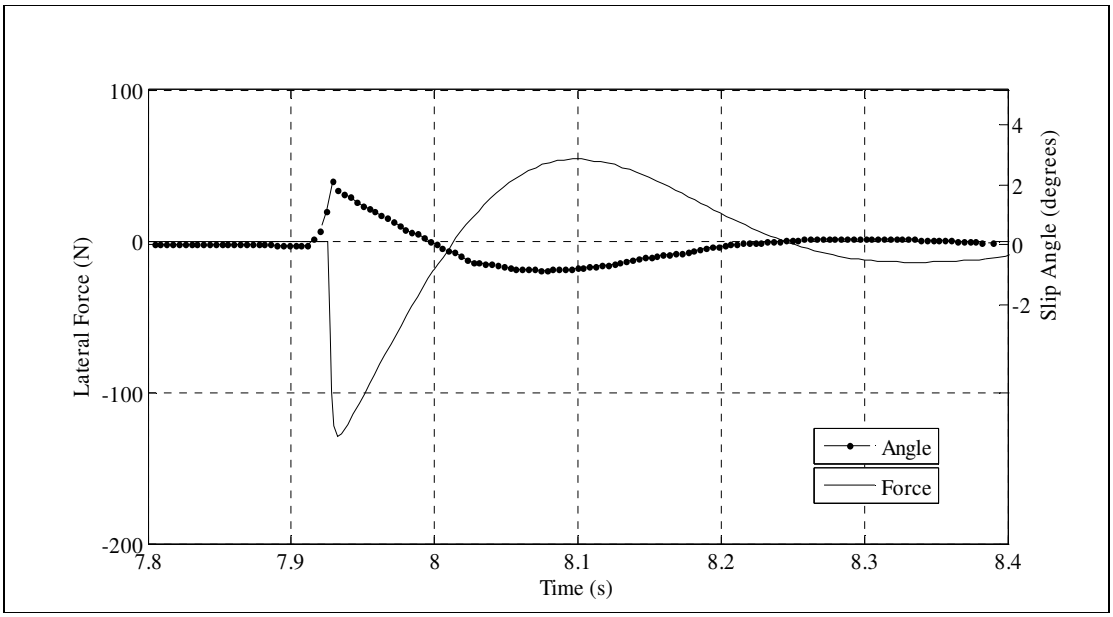

Figure 4. Front tyre slip angle and resulting lateral force

A peak lateral force of 187 N was measured at the rear tyre (primarily due to the greater vertical load of 383 N) together with a rear frame yaw velocity of 44 deg/s giving a peak power transfer of 73 W. The lower rear wheel power (despite greater lateral force generation) is due to both lower frame yaw velocity compared to front wheel yaw velocity and to peak yaw velocity occurring later in the cycle and thus not coinciding with peak force. Integrating rear wheel lateral power over the period gives work-done of 7.7 J which is closer to the front tyre value since integration eliminates the effect of the peak timing difference. Total lateral work-done as a consequence of steering input is 16.1 J, all of which would have been applied to forward bicycle propulsion if straight-running had been maintained.

7.6.2 Lateral Force due to Camber Angle

A peak front wheel camber angle of 2.9 degrees results from the steering input which generates 17 N of lateral force (Figure 5). This can be treated as additive to the slip induced lateral force while the tyre model relationships remain linear. Rear wheel camber angle of 4 degrees (Table 4) is somewhat greater than front wheel camber as it is not reduced by steering geometry effects. Additionally, a larger rear camber force of 27 N is found due to both the increased camber angle and the higher rear wheel camber stiffness reflecting the weight bias to the rear wheel. As a proportion of total lateral work-done, camber force contributes 16% compared to the slip force contribution of 84%. This relationship is consistent with findings for motorcycle tyres at low camber angles, but larger than the typical 5% camber force contribution to car tyre forces (Sharp [23]).

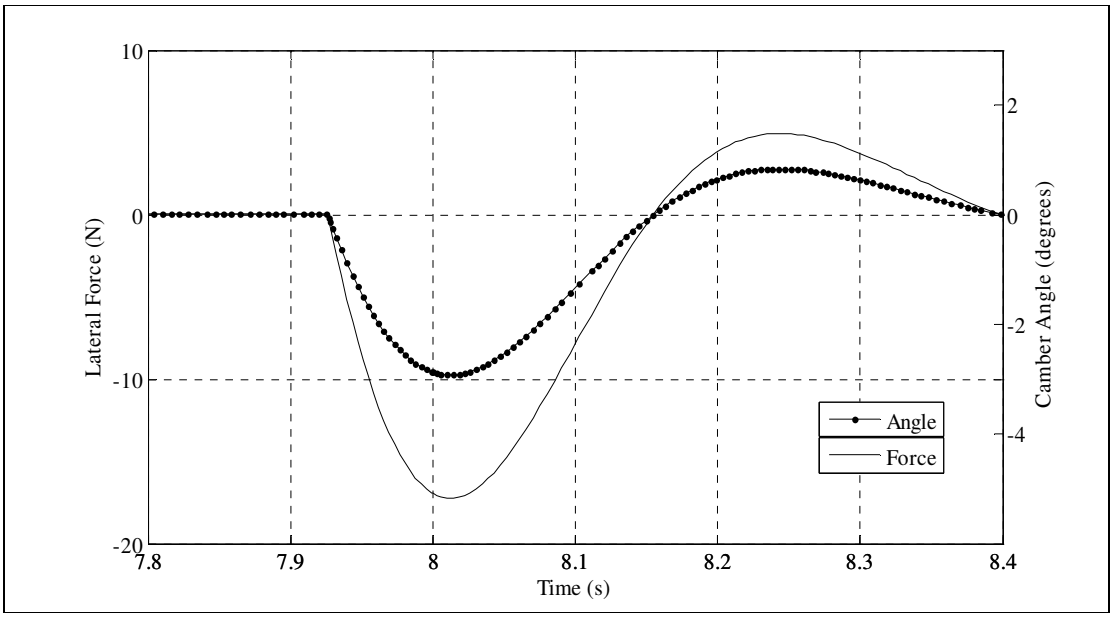

Figure 5. Front tyre camber angle and resulting lateral force

7.6.3 Further Analysis

The tyre model also measures and applies forces associated with wheel angular velocity (for power calculations), combined slip/camber force and aligning/overturning/rolling moments. Longitudinal slip from acceleration and braking is ignored due to the time trial context. Detailed results have been obtained but are not included here being beyond the scope of this paper.

7.7 Discussion

The main aims of this chapter are to quantify the forces and moments generated by a bicycle tyre model in response to steering input and confirm that they are realistic. A few studies have incorporated tyre models into bicycle handling simulations but have reported eigenvalues relating to bicycle self-stability rather than directly calculating tyre forces (Limebeer and Sharp [20]; Sharp [23]). Most bicycle field studies have been limited to measuring force and motion associated with the bicycle frame (e.g. steering angles and torques) as tyre forces can usually only be calculated indirectly from other instrumentation. However, Roland and Lynch [22] conducted field testing with a simplified tyre testing machine towed behind a car and reported a mean cornering stiffness of 60 N/degree at 3 degrees slip angle, 10 degrees camber angle and 330 N vertical load. Although not necessarily reproducing the response of a steered bicycle, the similarity of this result to the rear tyre force obtained in the current simulation (62N/deg at 3 degrees slip, 4 degrees camber and 338 N load) provides support for the validity of the tyre model, but with unresolved questions remaining on the contribution of camber to lateral force generation. Surprisingly, Roland and Lynch [22] show that camber thrust only contributes between zero and 33% of total lateral force when a 40 degree camber angle is applied. Further research is clearly needed to establish whether the approximately equal lateral force generated by 40° of camber and 3° of side-slip in motorcycles (Cossalter et al. [16]; Cossalter and Doria [27]) is applicable to the bicycle. However, it should be noted that there is some ambiguity in motorcycle data as Sharp [28] reports an estimated 80+% of lateral force at 50 degrees camber angle is attributable to camber thrust in a motorcycle simulation. Overall, the dynamics of bicycle tyres may be less similar to motorcycle tyres than has been supposed, possibly due to differences in dimensions/pressures and despite the common single-track characteristic.

An alternative approach to evaluating the reality of this study's results is to consider the effect of the total measured tyre force on performance. An important performance issue is the transfer of longitudinal propulsive power to lateral 'steering' power in the 'final sprint' scenario posed for this analysis. Such a power transfer would translate into loss of longitudinal position relative to 'non-steering' competitors and could loose a race for the instigator. The simulation found 19.6 J

of tyre propulsive work transferred to lateral work which was incurred between 7.92 s and 9 s when steady-state velocity was 11.1 m/s. During this period, total bicycle/rider work-done was 257 J and a distance of 11.9 m was covered suggesting that the propulsive loss of 7.63% (19.6/257*100) would equate to 0.9 m loss of longitudinal position. A typical bicycle wheelbase of 1 m makes this a loss of almost a bike length which would often equate to several places in a professional road race. The main conclusion from this analysis is therefore, not the exactitude of the position loss but rather that all the disparate force measurements by an 'un-tuned' bicycle model sum to a result that is believable in the context of real-world cycling.

8 INITIAL VALIDATION

8.1 Uncontrolled Stability Validation

8.1.1 Introduction

The first aim of this section is to validate the non-linear cycling model in so far as it reproduces the stability response of an uncontrolled bicycle reported by previous experimental and modelling studies. The second aim is to validate a linearised version of the cycling model by comparing stability mode eigenvalues with those reported by the 'benchmark' bicycle model of Meijaard et al. [4]. A recent study by Dressel [29] has made 'benchmark equivalent' equations of motion available for download (www.JBike6.com) together with software to manipulate the bicycle parameters before eigenvalues are calculated.

8.1.2 Methods

A sub-model was extracted from the complete cycling model to investigate uncontrolled stability and to compare the eigenvalues for the characteristic stability modes with those of the benchmark model. The model was first modified by reducing the rider to a rigid inert mass fixed to the rear frame. The investigation requires upright straight-running at a constant speed on a flat road so aerodynamic and gravitational resistive forces were removed and a constant velocity actuator was applied to the rear frame to 'launch' the bicycle at the required speed. The front and rear tire models were removed leaving each wheel with two non-holonomic constraints enforcing pure rolling (no-slip) conditions in the longitudinal and lateral directions. All constraints and actuators were removed leaving the bicycle with only freedom to translate longitudinally/laterally and roll/yaw/pitch/steer.

Ten separate simulations were run at velocities from 1 to 10 m/s at 1 m/s intervals and the resulting roll and steer profiles recorded to ascertain the bicycle stability characteristics. Simulation duration was 10 s (or less if terminated by a bicycle capsize). A lateral perturbation of 10 N was applied to the chain stay for 0.1 s after one second of straight-running. This force was applied directly above the rear contact point and therefore contributed only to roll. The model was then linearised for each velocity at an operating point 1.5 s into the simulation. Eigenvalues were extracted from the mass matrix of the resulting state-space representation and graphed for the real weave, imaginary weave, castoring and capsize modes. The JBike6 version of the benchmark model run was run over the same range of velocities with parameters that matched those of the bicycle in this study.

8.1.3 Results

The rider/bicycle was found to be self-stable from a velocity of 3.8 m/s to the limit of testing at 10 m/s. Above 3.8 m/s the roll and steer angle oscillations after perturbation gradually decayed until both exhibited close to zero values and upright equilibrium was restored (Figure 6). It was noted that the rate of roll and steer oscillation decay increased approximately linearly with velocity. In contrast, below 3.8 m/s the system exhibited increasing roll and steer oscillation leading to over-turning within eight seconds (Figure 7). The roll/steer oscillation period was 2.5 sec-

onds at 3 m/s with slower velocities increasing this period and thus advancing the onset of capsize.

The positive roll angles and negative steer angles in Figure 6 and Figure 7 show that the steering turned in the same direction as the roll. The steering response lags the roll by about 0.25 s at 3 m/s while the steering response is almost coincident with roll at 5 m/s. There was a notable reduction in the peak roll/steer angle response to perturbation from 5 degrees at 3 m/s to 0.05 degrees at 5 m/s.

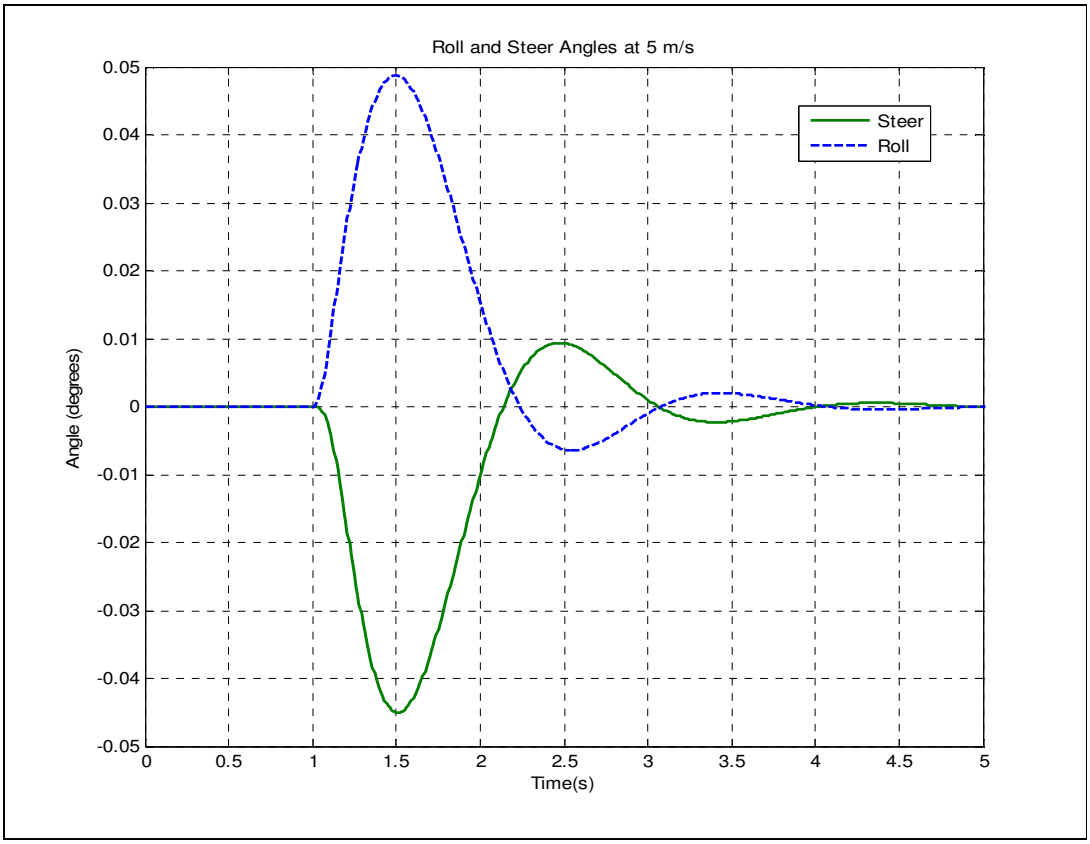

Figure 6. Roll and steer response to perturbation at a velocity of 5 m/s

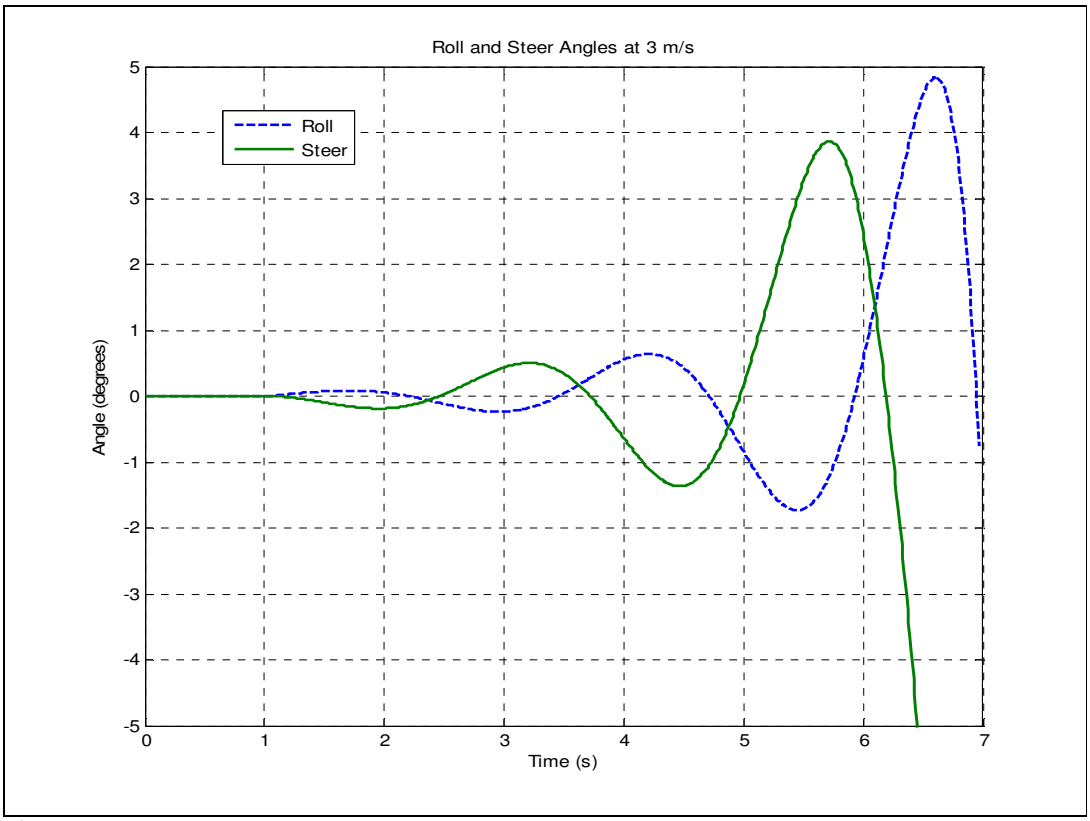

Figure 7. Roll and steer response to perturbation at a velocity of 3 m/s

In support of the above observations from the non-linear model, the linearised model eigenvalues calculated over the same speed range showed a similar self-stability window. The bicycle achieved low speed self-stability when the real weave mode eigenvalue changed from positive to negative at 3.8 m/s. However, no upper self-stability limit was found as the capsize mode eigenvalues remained negative over the tested speed range (Figure 8).

Comparing these results to the benchmark model, the eigenvalue plots show similar profiles for the real weave, imaginary weave and castering modes although the benchmark real weave zero crossing at 4.2 m/s is slightly higher than the 3.8 m/s for the cycling model. However, the benchmark model capsize at 6 m/s is significantly different from the cycling model which remained self-stable up to the maximum tested velocity of 10 m/s.

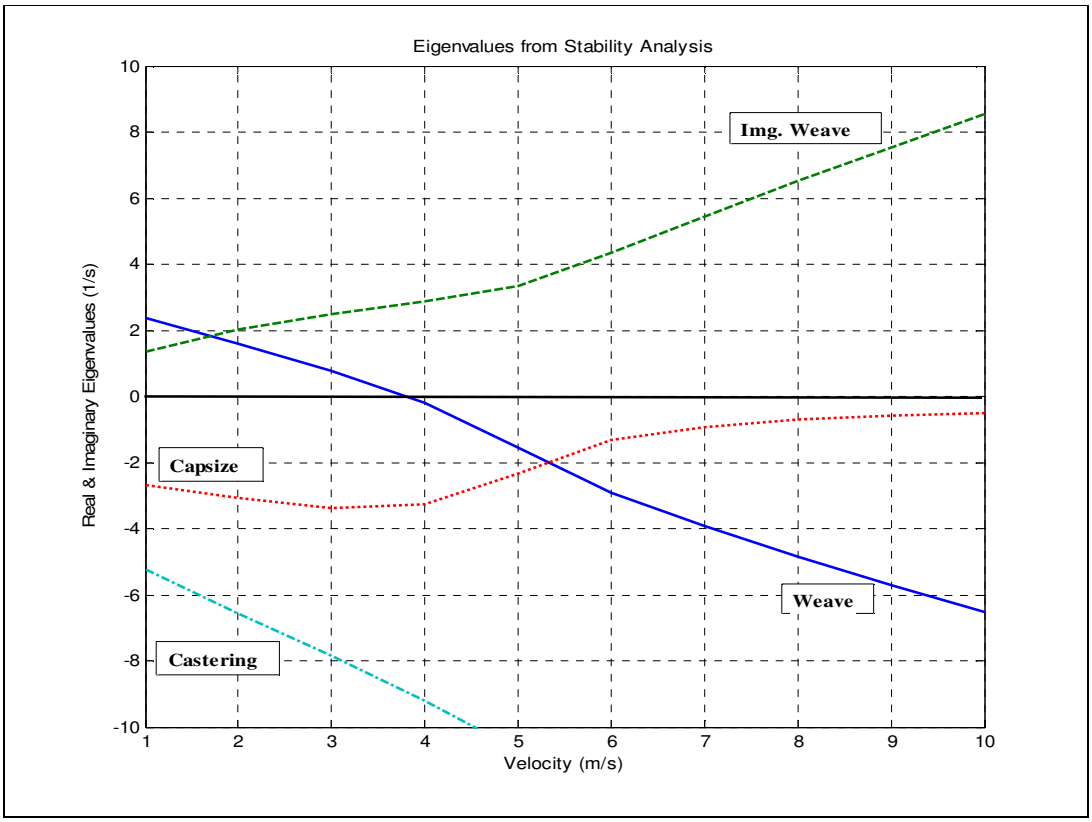

Figure 8. Eigenvalues representing stability modes obtained from the cycling model

8.1.4 Discussion

The first objective was to demonstrate that the model generated by SimMechanics produced uncontrolled stability responses consistent with the literature. This was achieved, with the graphs plotting roll and steer conforming to a typical transition from instability to self-stability at a velocity in the region of 4 m/s (Schwab et al. [30]; Limebeer and Sharp [20]). The steer response was in the same direction as the perturbation-induced roll to prevent a fall, which is largely a consequence of the steering geometry and the trail (Jackson and Dragovan [31]; Fajans [32]). The steering phase lag observed at lower velocities has been noted by other studies (Meijaard et al. [4]; Dressel [29]). Oscillation period of 1.6 seconds and phase lag of 0.1 seconds at 4.6 m/s were reported by Meijaard et al. [4] which are consistent with the values of 2.5 seconds and 0.25 seconds at this study's lower speed of 3 m/s. Steer/roll oscillation period and steer phase lag for a given velocity can be precisely calculated from the complex weave mode eigenvalues and eigenvectors (Dressel [29]).

The second objective sought to validate the cycling model by comparing the eigenvalues generated by a linearised version with those presented by the benchmark model. The castering mode eigenvalue was similar between the two models. The real weave eigenvalue exhibited a similar profile between the two models. A common zero crossing value would be the most significant similarity as it indicates the transition from oscillatory instability to bicycle self-stability. The difference of 0.5 m/s between the models is well within the variation that might be expected from the variances in design parameters (Dressel [29]).

The capsize mode is the only eigenvalue that is clearly different between the two models. The benchmark model shows it becoming positive at 6 m/s while the cycling model remains stable up to the 10 m/s test limit although, given the trend of the graph plot, it seems unlikely that zero crossing would have occurred even if the test range had been extended. However, it is apparent from examining eigenvalue graphs for similar bicycle configurations that the capsize mode has been reported to become positive over a particularly wide range of values. The experimental study of Kooijman et al. [33] reports a zero crossing at 7.9 m/s and also exhibits the curvilinear

capsize plot below 3 m/s which is seen in the cycling model. Dressel [29] with benchmark-equivalent equations of motion reports a zero crossing at 8 m/s while a separate study produced by a benchmark co-author (Schwab et al. [34]) reports zero crossing at ~7.896 m/s. This latter study also suggests that the positive capsize eigenvalue will again approach zero from above (i.e. become negative) as the speed increases further. In the same study, a hypothetical bicycle is modelled with zero trail and zero gyroscopic forces which shows the capsize mode remaining permanently negative. It is therefore apparent that the capsize mode zero crossing is dependent on bike geometry.

In conclusion the evidence presented in this study suggests that the cycling model generated by SimMechanics is a valid derivation of the equations of motion that represent a moving bicycle. The non-linear cycling model reproduces the roll and steer responses reported in the literature. Additionally, the linearised version reproduces the eigenvalues representing self-stability that have been reported by a benchmark model, with the exception that no upper limit velocity is observed although this may not be significant. The cycling model can therefore be considered numerically valid, laying a sound foundation for the next stage of experimental validation.

8.2 Crank Torque Validation

A benchmark mode in respect of pedalling torque profile on an ergometer has been presented in the literature by Redfield and Hull [6]. A static version of the pedalling rider model was created in this study to enable direct comparison with the benchmark. The crank torque profile over 360° correlated well (R^2=0.97) with the benchmark model when the rider pedalled at 255 W.

9 EXPERIMENTAL VALIDATION

9.1 Experimental Design

Fourteen experienced male time trial cyclists were recruited through articles in the national cycling press and internet cycling forums. Participants selected were representative of good club/national level competitors with a current time of 21-25 minutes for a 10 mile time trial. Participants were fully informed of the procedures and risks involved in the study before giving written informed consent. The study was approved by the university Ethics Committee. Trials were conducted on the first 2.5 miles of the Cycling Time Trials (CTT) course G10/42 near Dorking (UK) which is a straight, undulating dual-carriageway time trial course. Participants rode their own bicycle after each was fitted with a PowerTap SL power meter (Saris Cycling Group, Madison, WI) or an SRM power meter (Schoberer Rad Messtechnik GmbH, Julich, DE). Both systems utilise a handlebar mounted screen enabling current propulsive power to be viewed. All systems were calibrated before each trial in accordance with the manufacturer's instructions. The PowerTap gives a 1.2% lower power reading compared to the 'gold standard' SRM with power coefficients of variation (CV) of 1.8% and 1.5% respectively (Bertucci, Duc, Villerius, Pernin & Grappe [35]). Paton & Hopkins [36] reported similar power CV's of 1.5% for the PowerTap and 1.6% for the SRM but more importantly for this study, identified the mechanical component of the CV's as 0.9% and 1.1% respectively (equivalent to a ~0.4% speed error). These later values are applicable to this study as power control largely eliminated biological variation.

A digital representation of the course section was obtained from a mapping CD (Memory Map Europe, Aldermaston, UK) and the course track (latitude/longitude) and height profile entered into the model. The mean gradient is 3% with a peak of 9%, there are no appreciable flat parts and the start and finish are at the same height.

Each participant was tested separately on a single day starting with a warm-up/familiarisation. Testing was only conducted in good weather conditions (dry, wind <5 m/s) and a rolling start was implemented for all runs. The wind strength and direction was measured with an anemome-

ter (WindWorks, www.bythebeachsoftware.com) at a representative location on the course at the start and end of the day's trial.

The trial was completed at the participant's best self-selected 10 mile time trial pace in order to compare the resulting time with the model prediction for that individual. To enable this comparison, the model was parameterised with the individual, bicycle and environmental data in respect of mass, aerodynamic coefficient of drag area (CDA) and wind strength/direction. The CDA was computed from the product of cyclist/bicycle frontal area and a drag factor (Figure 9). Dependant on bicycle type, participants were divided into three categories comprising full T/T bike, road bike with tribars and road bike with 'hands on hoods'. Frontal area for each cyclist+bicycle was obtained by passing rider weight into the regression equations derived for each category by Heil [37] and Heil [38]. Drag factor was calculated from the product of aerodynamic factors obtained from wind tunnel testing for rider position, bicycle structure, bicycle components, clothing and helmet as presented in Bassett et al. [39]. Wind strength and direction are shown in Figure 9 with a zero direction indicating wind from due south and negative values indicating wind from the west.

9.2 Data Collection and Analysis

Time, power, speed and distance data for each trial were recorded on the power meter at ≈1 s intervals. To model predicted time for each individual, the recorded power profile for the trial was input to the model together with individual parameters for wind conditions, mass, and CDA.

9.3 Statistical Analysis

Data sets were checked for normality with a Shapiro-Wilks test and for equal/unequal residual variance with an F-Test. Data were analysed with a paired t-test to identify any significant difference between predicted and actual completion time and with linear regression to identify any relationship between predicted and actual completion time. All data were analysed with SPSS (SPSS Inc, Chicago, IL) with significance set at $p \leq 0.05$.

9.4 Results

The required assumptions for the statistical analysis were confirmed with data sets normally distributed ($p > 0.248$) and an F-Test showing unequal variances between data sets ($F > 1.194$, $p > 0.288$). The results are shown in Figure 9. Mean predicted and actual times for the 14 participants were 371 (±35) s and 366 (±32) s respectively. The mean 5 s reduction in actual time was significant ($t = -3.104$, $p = 0.008$) and demonstrated a model predictive error level of 1.4% (±1.5%). Actual and predicted times were closely related ($R^2 = 0.973$) and are shown in Figure 10.

ID	Height (m)	Cyclist Weight (kg)	Total Weight (N)	BSA (sq m)	Frontal Area[a]	Drag Coefficient	CDA	Wind Direction (rad)	Wind Speed (m/s)	Actual Time (s)	Predicted Time (s)	Predicted Variance (s)	Absolute Variance
1	1.73	71	765	1.84	0.30	0.83	0.25	-1.0	1.3	315	314	-1	0.3%
2	1.80	67	736	1.85	0.29	0.89	0.26	-0.8	2.2	335	349	14	4.2%
3	1.80	70	755	1.89	0.30	0.84	0.25	-0.7	1.5	354	356	2	0.6%
4	1.83	79	844	2.01	0.32	0.78	0.25	-1.2	3.9	346	348	2	0.6%
5	1.85	79	844	2.03	0.32	0.78	0.25	-0.8	1.7	336	336	0	0.0%
6	1.78	81	863	1.99	0.33	0.80	0.26	-0.4	2.9	350	354	4	1.1%
7	1.82	69	765	1.89	0.44	0.69	0.30	-1.1	3.3	401	402	1	0.2%
8	1.78	73	795	1.90	0.45	0.66	0.30	-0.7	2.0	372	377	5	1.3%
9	1.67	64	716	1.72	0.42	0.77	0.32	-0.2	3.0	401	421	20	5.0%
10	1.83	93	990	2.15	0.52	0.65	0.34	-0.6	2.0	378	381	3	0.8%
11	1.85	82	893	2.06	0.59	0.59	0.35	-1.2	1.4	355	360	5	1.4%
12	1.81	78	800	1.98	0.58	0.64	0.37	-0.7	2.1	375	384	9	2.4%
13	1.80	80	820	2.00	0.58	0.63	0.37	-0.7	3.4	440	446	6	1.4%
14	1.80	83	810	2.03	0.60	0.62	0.37	-0.7	1.3	370	369	-1	0.3%

Figure 9. Individual Data and Results. (Frontal Area[a] . ID 1-5. Full T/T bike (Heil, 2005). ID 7-10. Road Bike Tribars (Heil, 2002). ID 11-14. Road Bike Hoods (Heil, 2002))

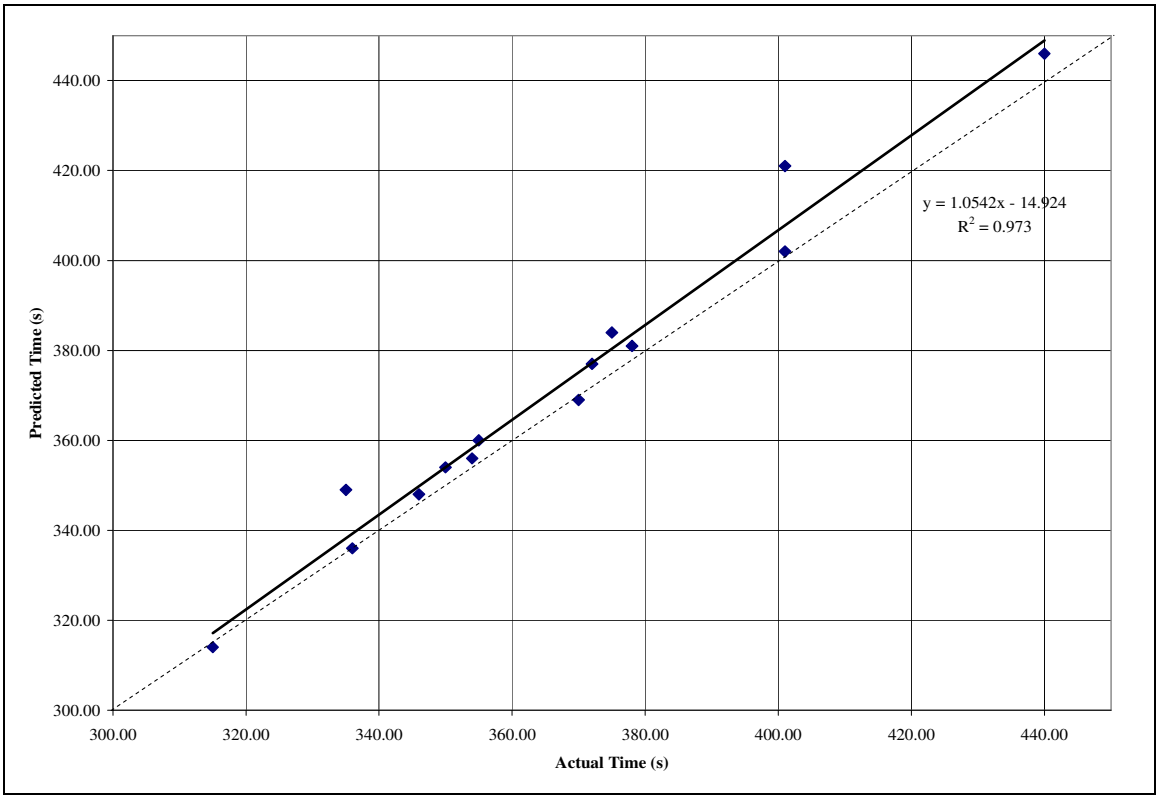

Figure 10. Regression analysis of individual times

9.5 Discussion

The objective of experimental validation was to compare the time achieved by an individual in a field time trial with the time predicted for that individual by the model. The model predicted individual rider time was 1.4% higher than the actual time. This compares well with the average error of 1.32% reported by the only two comparable models which combine first principles with road cycling (Martin et al. [12]; Olds et al. [10]). Comparison with Martin et al. [12] must be indirect as the measured dependant variable was power rather than completion time. However, it

can be calculated from the presented data (for the 11 m/s trials which are equivalent to this study) that the average model predicted time over the equivalent distance was 3.3 s faster than the actual time of 365 s giving a 0.9% error. This compares well with the 366 s actual time and 1.4% error in this study although the time agreement is likely to be coincidental as their course was flat (0.3% gradient) and straight. Martin et al. [12] also found that model predicted time was faster than actual time which is the reverse of this study. In part, this may reflect the absence of a traffic 'towing' effect on their closed airfield course. Olds et al. [10] compared model predicted and actual times for 41 cyclists over a 26 km flat (<0.5% gradient) course. The mean model predicted time was 0.74 min greater than the actual time of 42.8 min giving an error level of 1.73%, similar to the 1.4% found in this study. However, Olds et al. [10] reported a large error SD of ±2.07 min and range of +5.56 to -3.15 min which they attributed to less accurate modelling of the sixteen recreational cyclists included in the sample.

In conclusion, the experimental validation suggests that the model is an accurate representation of road time trial cycling. Specific kinematic and kinetic variables were not measured during the time trial for comparison with modelled values but it seems unlikely that accumulated errors would sum to a valid result. However, it must be accepted that the validation was specific to a particular time trial course and conditions which may not hold true for all road cycling. Further studies with measuring devices fitted to the bicycle will be needed if the model validity is to be extrapolated to a wider range of conditions.

10 SUMMARY

This study has described a comprehensive model of road cycling which combines the bicycle, rider and environment in a single dynamic system. The model can be parameterised with rigid body and course characteristics and actuated with force or motion profiles to simulate competitive field cycling. A variable step ODE solver integrates output that can be used to evaluate the effect of tuning mechanical variables on cycling performance. The model has been validated with reference to existing models in the literature and by comparing predicted completion time over a time trial course with field experiment data

Further studies with the validated model are planned to investigate the mechanical performance advantages of bike/rider weight, saddle position, crank length, tyre characteristics and the contribution of muscular/non-muscular forces to pedalling.

REFERENCES

[1] F. J. W. Whipple, "The Stability of the Motion of a Bicycle.," *The Quarterly Journal of Pure and Applied Mathematics* **30** (1899), pp. 312-348.

[2] M. E. Carvallo, "Théorie du mouvement du Monocycle et de la Bicyclette," *Journal de L'Ecole Polytechnique* **5** (1900), pp. 119-188.

[3] R. D. Roland, "Computer simulation of bicycle dynamics.," *Proceedings of the ASME Symposium Mechanics and Sport* (1973), pp. 35-83.

[4] J. P. Meijaard, J. M. Papadopoulos, A. Ruina, and A. L. Schwab, "Linearized dynamics equations for the balance and steer of a bicycle: a benchmark and review," *Proceedings of the Royal Society of London* **A463** (2007), pp. 1955-1982.

[5] M. L. Hull and M. Jorge, "A method for biomechanical analysis of bicycle pedalling," *Journal of Biomechanics* **18** (1985), pp. 631-644.

[6] R. Redfield and M. L. Hull, "On the relation between joint moments and pedalling rates at constant power in bicycling," *Journal of Biomechanics* **19** (1986), pp. 317-29.

[7] R. R. Neptune and M. L. Hull, "Evaluation of performance criteria for simulation of submaximal steady-state cycling using a forward dynamic model," *Journal of Biomechanical Engineering* **120** (1998), pp. 334-341.

[8] P. D. Soden and B. A. Adeyefa, "Forces applied to a bicycle during normal cycling," *Journal of Biomechanics* **12** (1979), pp. 527-41.

[9] C. Stone and M. L. Hull, "The effect of rider weight on rider-induced loads during common cycling situations," *Journal of Biomechanics* **28** (1995), pp. 365-375.
[10] T. S. Olds, K. I. Norton, E. L. Lowe, S. Olive, F. Reay, and S. Ly, "Modeling road-cycling performance," *Journal of Applied Physiology* **78** (1995), pp. 1596-1611.
[11] D. P. Swain, "A model for optimizing cycling performance by varying power on hills and in wind," *Medicine and Science in Sports and Exercise* **29** (1997), pp. 1104-1108.
[12] J. C. Martin, D. L. Milliken, J. E. Cobb, K. L. McFadden, and A. R. Coggan, "Validation of a Mathematical Model for Road Cycling Power," *Journal of Applied Biomechanics* **14** (1998), pp. 276-291.
[13] M. Bailey, X. Nesi, L. Passfield, and H. Carter, "Comparison of cycle crank torque computed from forces applied to the pedals and measured with an SRM ergometer.," *Proceedings of the European College of Sport Science Congress* (2006), pp. July 5th - 8th, Lausanne, Switzerland.
[14] C. R. Kyle, "Energy and aerodynamics in bicycling," *Clinics in Sports Medicine* **13** (1994), pp. 39-73.
[15] G. E. Caldwell, L. Li, S. D. McCole, and J. M. Hagberg, "Pedal and Crank Kinetics in Uphill Cycling," *Journal of Applied Biomechanics* **14** (1998), pp. 245-259.
[16] V. Cossalter, A. Doria, R. Lot, N. Ruffo, and M. Salvador, "Dynamic Properties of Motorcycle and Scooter Tires: Measurement and Comparison.," *Vehicle System Dynamics* **39** (2003), pp. 329-352.
[17] R. Lot, "A Motorcycle Tire Model for Dynamic Simulations: Theoretical and Experimental Aspects," *Meccanica* **39** (2004), pp. 207-220.
[18] H. B. Pacejka, *Tyre and Vehicle Dynamics*. Oxford, UK: Butterworth-Heinemann, 2002.
[19] J. P. Meijaard and A. L. Schwab, "Linearized equations for an extended bicycle model.," *European Conference on Computational Mechanics* (2006), pp. 1-18.
[20] D. J. N. Limebeer and R. S. Sharp, "Bicycles, motorcycles and models.," *IEEE Control Systems Magazine* **36** (2006), pp. 34-61.
[21] D. J. Cole and Y. H. Khoo, "Prediction of vehicle stability using a 'back to back' tyre test method," *International Journal of Vehicle Design* **26** (2001), pp. 573-582.
[22] R. D. Roland and J. P. Lynch, "Bicycle dynamics tire characteristics and rider modeling.," *Cornell Aeronautical Laboratory* (1972), pp. Report no. YA-3063-K-2.
[23] R. S. Sharp, "On the stability and control of the bicycle.," *Applied Mechanics Reviews* **61** (2008), pp. 1-24.
[24] C. R. Kyle, "Selecting Cycling Equipment," in *High-Tech Cycling*, E. R. e. Burke, Ed., 2nd Edition ed. Champaign, IL: Human Kinetics, 2003, pp. 1-48.
[25] T. D. Gillespie, *Fundamentals of Vehicle Dynamics.* Warrendale, PA: SAE, 1992.
[26] M. Blundell and D. Harty, *The Multibody Systems Approach to Vehicle Dynamics.* Oxford, UK: Butterworth-Heinemann, 2004.
[27] V. Cossalter and A. Doria, "The relation between contact patch geometry and the mechanical properties of motorcycle tyres.," *Vehicle System Dynamics* **43** (2005), pp. 156-164.
[28] R. S. Sharp, "Motorcycle steering control by road preview," *Journal of dynamic systems, measurement, and control* **129** (2007), pp. 373-381.
[29] A. Dressel, "The Benchmarked Linearized Equations of Motion for an Idealized Bicycle.," *http://ecommons.library.cornell.edu/handle/1813/3615?mode=full* (2007), pp. Ph.D. Thesis.
[30] A. L. Schwab, J. P. Meijaard, and J. M. Papadopoulos, "Benchmark Results on the Linearized Equations of Motion of an Uncontrolled Bicycle.," *International Journal of Mechanical Science and Technology* **19** (2005), pp. 292-304.
[31] A. W. Jackson and M. Dragovan, "An experimental investigation of bicycle dynamics," *American Journal of Physics* **68** (2000), pp. 973-978.
[32] J. Fajans, "Steering in bicycles and motorcycles.," *American Journal of Physics* **68** (2000), pp. 654-659.
[33] J. D. G. Kooijman, A. L. Schwab, and J. P. Meijaard, "Experimental validation of a model of an uncontrolled bicycle," *Multibody System Dynamics* **19** (2008), pp. 115-132.

[34] A. L. Schwab, J. P. Meijaard, and J. D. G. Kooijman, "Some recent developments in bicycle dynamics.," *Proceedings of the 12th World Congress in Mechanism and Machine Science* (2007).

[35] W. Bertucci, S. Duc, V. Villerius, J. N. Pernin, and F. Grappe, "Validity and reliability of the PowerTap mobile cycling powermeter when compared with the SRM Device," *International Journal of Sports Medicine* **26** (2005), pp. 868-873.

[36] C. D. Paton and W. G. Hopkins, "Ergometer error and biological variation in power output in a performance test with three cycle ergometers," *International Journal of Sports Medicine* **27** (2006), pp. 444-447.

[37] D. P. Heil, "Body mass scaling of frontal area in competitive cyclists not using aero-handlebars," *European Journal of Applied Physiology* **87** (2002), pp. 520-528.

[38] D. P. Heil, "Body size as a determinant of the 1-h cycling record at sea level and altitude," *European Journal of Applied Physiology* **93** (2005), pp. 547-554.

[39] D. R. Bassett, Jr., C. R. Kyle, L. Passfield, J. P. Broker, and E. R. Burke, "Comparing cycling world hour records, 1967-1996: modeling with empirical data," *Medicine and Science in Sports and Exercise* **31** (1999), pp. 1665-1676.